

# Morphology of Proliferating Epithelial Cellular Tissue

Pranav Madhikar

*Department of Mathematics and Computer Science & Institute for Complex Molecular Systems,  
Eindhoven University of Technology, 5600 MB, Eindhoven, Netherlands*

Jan Åström

*CSC Scientific Computing Ltd, Kägelstranden 14, 02150 Esbo, Finland*

Björn Baumeier

*Department of Mathematics and Computer Science & Institute for Complex Molecular Systems,  
Eindhoven University of Technology, 5600 MB, Eindhoven, Netherlands*

Mikko Karttunen

*Department of Chemistry and Department of Applied Mathematics,  
Western University, 1151 Richmond Street, London, Ontario N6A 5B7, Canada*

(Dated: November 16, 2018)

We investigate morphologies of proliferating cellular tissue using a newly developed numerical simulation model for mechanical cell division. The model reproduces structures of simple multicellular organisms via simple rules for selective division and division plane orientation. The model is applied to a bimodal mixture of stiff cells with a low growth potential and soft cells with a high growth potential. In an even mixture, the soft cells develop into a tissue matrix and the stiff cells into a dendrite-like network structure. For soft cell inclusion in a stiff cellular matrix, the soft cells develop to a fast growing tumour like structure that gradually evacuates the stiff cell matrix. With increasing inter-cell friction, the tumour growth slows down and parts of it is driven to self-inflicted cell death.

Morphology and dynamics of proliferating cells are among the fundamental issues at different stages of cellular development [1–6]. They are controlled by a number of factors, but from the physical point of view, morphology is tightly coupled to inter-cellular force transmission, see e.g., Refs. [6–8]; mechanical forces have been shown to be important in cancer development and it has been suggested that tumour growth may even be arrested by inter-cellular mechanical forces [9, 10]. Among the many complications in investigating force transmission are that at their embryonic state, cells may not yet have developed junctions and may display more fluid-like behaviour, and that cell-cell adhesion depends on the cell types [7, 11–13]. Junctions are crucial in cell-to-cell stress transmission [7, 8, 14, 15] but it is, however, challenging to probe the individual junctions experimentally.

From a coarse-grained point of view, that is, ignoring chemical details and treating cells as elastic objects, cellular systems can be seen as disperse grand canonical soft colloidal systems under evolving pressure applied non-uniformly throughout the system. Several studies have tried to capture aspects of growing soft colloidal systems (e.g. for modelling tissue growth) at different levels [16–19] but even in simple systems many fundamental questions remain open including the precise nature of colloidal phase diagrams when colloids are soft with size dispersity [20], and structure selection via self-assembly [21]. Cellular systems are more complex since they exhibit additional behaviours such as cell growth and division, they have varying mechanical properties (e.g. elasticity and cell-cell adhesion) and their response to external stimulus may be sensitive to the local environment.

Dimensionality has an important role in particular in regulation of intra- and inter-cellular forces at different levels, see e.g. Refs. [22–26]. Some systems, such as epithelial tissues and *Drosophila* wing discs, are inherently two dimensional which gives them distinct morphological properties due to the nature of cellular packing, and transmission of and response to forces [5, 13, 27]. In addition, jamming can be very strong in two dimensional systems and varying stiffness and inter-membrane friction is a step towards investigating jamming in cellular systems [28, 29]. Our main focus is on the above effects in systems consisting of hard cells in a soft matrix and vice versa. Besides being important in understanding the mechanisms of cell movement under pressure [8], such situations have been proposed to be important in tumour growth [9, 10] – cancer cells are often softer than healthy cells [30, 31] although the opposite has also been reported [32, 33]. Cell stiffness, its measurements and connection to cancer metastasis have been recently reviewed by Luo et al. [34].

One of the intriguing questions in cell division is: Why do cells exhibit diverse morphologies upon division and growth? In addition to uniform structures, a plethora of structures with various mechanisms and division modes have been suggested but the issue remains largely unresolved [13, 39–41]. To illustrate how different morphologies can arise, consider cyanobacteria. Figures 1a)–c) show *Anabanea circinalis* and Fig. 1d) *A. flos-aquae*. Both of them can be approximated as quasi one-dimensional structures. In contrast to most other cells, however, cyanobacteria have continuous outer membranes shared by the whole filament consisting of multiple cells [41, 42]. The inner membranes, however, belong to individual bacteria only. It has been suggested that this together with specialized junctions leads to filamentous structures (there are also subtleties related to, e.g., size selection of the filaments) [41, 42].

In our previous study [43], the orientation of the division line was selected randomly. The simplest way to model cyanobacteria morphologies is to choose the orientation of the division plane in such a way that it is approximately parallel between neighbouring cells. Although an approximation, this approach should be able to produce similar morphologies.

Typically, two dimensional systems exhibiting uniform non-directional growth have been studied

using vertex models, see, e.g. Refs. [44–46] and Refs. [17, 47] for reviews. One dimensional systems, however, have gained lesser attention and the models are typically of reaction-diffusion type with fixed geometry and size as discussed extensively in the review by Herrero et al. [41]

We employ the two-dimensional CeDEM (the Cellular Discrete Element Model) to investigate tissue morphologies in one and two dimensions. Full details and derivation of the model are provided in Ref. [43] but to summarize, in CeDEM the cell membrane is discretized as beads connected by bonds of stiffness  $K_i^{\text{spr}}$ .

Cellular growth is controlled by a growth pressure and division by a threshold in cell area (above which cells divide) and the orientation of the cell division line. Importantly, CeDEM allows the topology (the polygonal distribution) to vary spontaneously [43].

Here, we extend CeDEM for simulations of different cell types using three simple approaches:

1. changing the cell division line orientation,
2. changing cell stiffness, and, finally,
3. changing the friction between cell membranes; in CeDEM cell membrane and cytoskeleton are treated as a coarse-grained single object.

In our previous study, the orientation of the division line of each cell was chosen randomly and it was constrained to pass through the centre of mass of the cell undergoing division. This results in tissue growth such that it fills the available space roughly uniformly [43]. Modification 1) above allows for simulations of cyanobacteria-like structures shown in Fig. 1.

Modification 2) allows for simulations of different types of cells. As mentioned above, cancer cells typically considered to be softer than the matrix cells. Softness, or higher malleability, is typically associated with the invasiveness of cancer cells [34]. This has recently been challenged by Nguyen [33] et al. who measured Young’s modules of pancreatic cancer cells using different cell lines and found the stiffer (than the matrix cells) cells to be more invasive than the softer cancer cells. Whether this is purely mechanical or due to simultaneously occurring biological processes remains unclear. Here, we use two types: 1) *Type1*, stiff cells with a low growth potential with stiffness  $K_1^{\text{spr}}$ . The low growth potential means that the cell membrane is so stiff that the applied pressure is barely enough to grow the cell to a size above the division threshold. Therefore, if the cell is even lightly squeezed between other cells it will not divide before force equilibrium is reached and growth stops. 2) *Type2*, soft cells with a high growth potential with stiffness  $K_2^{\text{spr}}$ . These cells have a high growth potential which means that cell membrane stiffness is so low that the cell area easily grows beyond the division size. The cells are identical in all other ways except their stiffness.

Finally, modification 3) allows for comparisons of systems of cells with different inter-membrane friction coefficients. Cell-cell friction and its importance in mechanotransduction has recently been reviewed by Angelini et al. [48]. Inter-membrane friction is modelled as

$$\vec{F}_i^{\text{ext}} = -\mu \vec{v}_{ij},$$

where  $\mu$  is the friction coefficient and  $\vec{v}_{ij}$  is the component of the relative velocity between two membranes tangential to the cell that bead  $i$  belongs to. We compare systems where  $\mu = 0.0$ , that is, cells do not interact very much with their neighbours, and strongly interacting cells with  $\mu = 20.0$ .

## RESULTS

### Quasi-one-dimensional morphology

We start from (quasi-) one-dimensional systems and compare the structures from experimental systems (Fig. 1) and simulations (Fig. 2). First, instead of just dividing all cells that are above some threshold area, we allow a single cell to divide only once. Thus, only the youngest cells are allowed to divide similar to budding growth in bacteria [49]. Additionally, we make the division plane non-random. Different scenarios lead to morphologies as shown in Fig. 2: Keeping the division plane parallel for each generation leads to morphologies similar to *A. planctonica* (compare Figs. 1a and 2a). Letting the division line rotate slightly more by every generation produces Fig. 2b. Allowing all cells to divide and letting them divide along two perpendicular lines produces Fig. 2c, approximating the morphology of *A. laxa* in Fig. 1b. Finally, constant rotation every generation leads to Fig. 2d, which is structurally similar to Figs. 1b and 1d.

Although the morphologies in Fig. 2 are created by the simple rules as discussed above, and there may well be other rules that lead to similar morphologies, it is important to keep in mind that to arrive to such structures real systems have molecular mechanisms that lead to the emergence of such structures. The microscopic molecular level mechanisms are effectively manifested as rules at the macroscopic level. The exact mechanisms as why filamentous shapes form remain to be resolved, but current evidence shows that septal junctions have an important role [41, 50].

### Soft and stiff cells in 2D

We now focus on two-dimensional larger and denser samples of cells with two cell types, stiff (*Type1*) and soft (*Type2*), in the same system. We assume that softer cells are tumour cells. This assumption is based on the fact that cancer cells tend to be softer [30, 31]. The initial setups for simulations of such systems were created with equal proportions of *Type1* (red) and *Type2* (blue) cells, see Figure 3a). Growth is simulated with identical parameters for all cells, except membrane stiffness, until confluence. Figure 3b) shows the tissue structure at the end of the simulation with the system mostly filled with soft cells (blue) while the stiff cells (red) are compressed into dendrite-like structures. Another distinct feature is that the cells interpenetrate in the regions marked with light purple in Fig. 3b). This type of behaviour occurs in diverse systems as shown by Eisenhoffer *et al.* for canine, human and zebrafish epithelial cells [51] and discussed at length in the review by Guillot and Lecuit [13] (see in particular Fig. 2 in Ref. [13]). The forces can become so high that the cell membranes practically intersect each other. These cells would be good candidates for cell death. Experiments have also suggested that for live cells, such conditions may lead to pathologies [51]. CeDEM does not currently support cell death in terms of cells disintegrating and disappearing from the system. Cells do, however, get squeezed into very small space and division ceases in the purple regions of Fig. 3b).

Figure 3c) shows a smoothed histogram of the average inter-membrane (or contact) forces between cells. The white dots show the centres of masses of the stiff cells. The peaks in the contact force distribution correlate highly with the locations of the stiff cells indicating that *Type2* cells overwhelm *Type1* cells as the tissue grows and also that the system imposes higher stresses on the stiff collapsed cells.

At this point, we ask the question if this collapse of stiff cells can be mitigated by making their

interactions stronger. This can be examined by changing the magnitude of inter-membrane friction  $\mu$ . Since cells need to find space to grow, they need to slide past each other into empty regions. In other words, higher friction induces jamming between the cells which means that they easily get squeezed between each other and therefore reaching the division threshold area takes a much longer time. The softer cells will also need to counteract this effect to grow. Figure 4 shows a similar simulation setup as before, except with different values of  $\mu$ . Figure 4a) shows the initial conditions, and Figs. 4b) and c) show the final state at  $\mu = 0.0$  and  $\mu = 20.0$ , respectively.

At low inter-membrane friction ( $\mu = 0.0$ ), there are more cells at the end of the simulation indicating that growth is faster. The high inter-membrane friction system ( $\mu = 20.0$ ) is more porous with slower growth. The friction-less system (Fig. 4a)) corresponds to very early stages of development when junctions have not yet developed. The latter system corresponds (Fig. 4b)) to when cell adhesion molecules have developed. In both cases, the simulations were run for interval of time corresponding to 10 division cycles.

To investigate further, we study the sizes of the cells in each case and the forces that are acting on the cells. Figure 5 shows the number distributions of cell area (Fig. 5a)) and the total force (attractive, repulsive, and friction) that each cell feels due to its neighbours (Fig. 5a)). Both distributions display lower total number of cells in the high friction tissue. The peak in area distributions is just below 1.0, which is due to the threshold division area ( $A^{div} = 1.0$ ). Some of the cell areas have grown past this limit as cell division occur only at discrete time intervals in CeDEM so some cells are larger. The  $\mu = 0$  distribution shows a small peak at  $A \approx 0.2$ , which is due to the higher number of collapsed cells in the low friction system. The large-area peak represents the soft-cell majority, and its shape is approximately Gaussian, consistent with the observation from simulations of non-dividing soft colloids [16]. For  $\mu = 20.0$  the distribution has not yet developed two peaks and there are some cells that can grow rapidly in the sparse areas of the packing.

Finally, we study the case of a cluster of soft cells inside a matrix of stiff cells, Figure 6. We first investigate the case when  $\mu = 0.0$ . In this case, *Type2* cells with the larger growth potential continue to proliferate even when the tissue approaches the state of being space-filling, while *Type1* proliferation almost stops. This leads to a tumour-like growth of *Type2* cells and compression of *Type1* cells at the tumour boundary.

Figures 6a) and b) show the initial configurations of this type of simulation for  $\mu = 0.0$  and  $\mu = 20.0$ . Figures 6c) and d) show the morphologies for each case at confluence. The faster growth of the tumour at  $\mu = 0.0$  is clearly visible. Figures 6e) and f) show spatial size distributions in the two cases. The dark regions in the histograms correspond to pores in the system. Cell sizes are roughly equal within the tumour and inside the matrix. Along the tumour boundary, however, the matrix cells are compressed and the tumour cells are enlarged. This effect is seen in both cases but is much more pronounced when  $\mu = 0.0$ . Lastly, Figures 6g) and h) show the distribution of the mean contact forces. Inside the tumour the contact forces are low, and the largest forces are seen scattered on the tumour boundary. Again this effect is more pronounced in the  $\mu = 0.0$  case. However, even though there are fewer stressed cells at higher  $\mu$ , the few cells that are stressed feel higher stresses. This is quantified in Figures 7a) and b) which show the population distribution over contact force. In both of the current cases we see an exponential tail representing the small population of stressed cells at the tumour boundary. There are more cells that feel higher stress in Fig. 7a) with  $\mu = 0.0$ , than in Fig. 7b) with  $\mu = 20$ . However, these cells feel more stress at higher inter-membrane friction.

There is only very limited amount of data available for force distributions in proliferating systems. However, they have been measured for soft colloidal systems under compression. It is

well established that the distribution has an exponential tail in the vicinity of the jamming transition [16, 52, 53]. It has also been recently shown experimentally by Jose et al. by using 3-dimensional packings of soft colloids that the distribution well above the jamming distribution becomes Gaussian [52]. As Fig. 7 shows, the exponential tail is present in our two-component 2-dimensional cell systems both at zero and high friction. The fact that the cells grow also means that their volumes are not conserved (in contrast to experiments with typical colloids). This is also the case for the cells that are being pushed and compressed by their neighbours as is evident from the snapshots in Figs. 4 and 6. What is clearly different here is the distribution at low forces: the exponential is preceded by a Gaussian distribution. Gaussian peak has been observed in simulations of soft colloids in two dimensions with zero friction [16]. In contrast, in the three dimensional experiments of Jose et al. the low force part of the distribution remained almost flat except well above jamming transition. This may have to do with the hardness of the particles: Erikson et al. studied materials of different hardness and the force distribution at lower forces depends strongly on hardness [53]. In addition, van Eerd et al. have reported faster than exponential decay from their high accuracy Monte Carlo simulations [54] although the deviations can be very hard to detect without high accuracy sampling methods.

Here, peaks in the distribution that develop at relatively large forces within the bodies of stiff cells. This becomes particularly evident when a tissue of soft and stiff cells becomes so dense that it approaches space-filling. In this case, almost all stiff cells collapse and form narrow veins or dendrites. With a suitable initial mixture of stiff and soft cells, the soft cells form a matrix with a percolating fractal network of stiff cells which covers only a small fraction of the total area but penetrates almost everywhere (Fig. 3b)). This shows a possible pathway for the formation of signalling and transport networks in a simple multi-cellular system.

The results in Figure 6 show that the softer cells introduced into matrices of stiffer cells grow faster when inter-membrane friction is low; weaker cell-cell interactions provide conditions for easier growth. This also suggests that inter-cellular interactions can be an indicator of how well epithelial tissue can diminish the growth of rogue cells that have a higher growth potential.

## CONCLUSIONS

In this work we use the CeDEM model to study how filamentous growing bacteria can create varied quasi-one-dimensional morphologies. We show that modulating the cell division line orientation can be one of the ways such morphologies can arise. What determines the division line orientation is, however, an open question but cell-cell junctions have been indicated having an important role [41]. We propose considering simple division line placement rules as a possible effective manifestation of yet unknown microscopic mechanisms.

We then studied larger, denser systems of cells of two different types in two dimensions. Cell populations are differentiated by their membrane/cortex stiffness. We showed that this simple difference is enough, provided internal pressure is identical for both, to favour soft cell growth. Even if a few soft cells are introduced into a matrix of stiff cells, it is enough for the softer cell to grow rapidly. This effect can be mitigated by a higher interaction strength between cells. Both of the effects above required some modifications of the CeDEM model presented before in Refs. [16, 43]. We also studied the force distributions which shows similarities to non-proliferating soft colloidal systems. Although not studied here in detail, the model allows for tuning the cell-cell friction, an issue that recently been raised by Vinuth and Sastry for shear jamming [55].

The existing paradigm for the softness of cancer cells has been challenged by Rowat and coworkers who have shown that stiff cancer cells can be more invasive than soft ones [33]. They have also shown that cells experience significant strain hardening. The precise role of it remains to be resolved [56]. Models such as the current one may be helpful in isolating and identifying the purely mechanical processes and their importance for a collection of cells and related them to other soft matter systems.

## ACKNOWLEDGEMENTS

MK would like to thank the Discovery and Canada Research Chairs Programs of the Natural Sciences and Engineering Research Council of Canada (NSERC) for financial support.

- 
- [1] E. Paluch and C.-P. Heisenberg, *Curr. Biol.*, 2009, **19**, R790–R799.
  - [2] Y. Li, H. Naveed, S. Kachalo, L. X. Xu and J. Liang, *PLoS One*, 2012, **7**, e43108.
  - [3] C.-P. Heisenberg and Y. Bellaïche, *Cell*, 2013, **153**, 948–962.
  - [4] K. Ragkousi and M. C. Gibson, *J. Cell. Biol.*, 2014, **207**, 181–188.
  - [5] W. T. Gibson, B. Y. Rubinstein, E. J. Meyer, J. H. Veldhuis, G. Brodland, R. Nagpal and M. C. Gibson, *Theor. Biol. Med. Model.*, 2014, **11**, 26.
  - [6] D. Sanchez-Gutierrez, M. Tozluoglu, J. D. Barry, A. Pascual, Y. Mao and L. M. Escudero, *EMBO J.*, 2015, **35**, 77–88.
  - [7] M. Rauzi, P. Verant, T. Lecuit and P.-F. Lenne, *Nat. Cell. Biol.*, 2008, **10**, 1401–1410.
  - [8] D. T. Tambe, C. C. Hardin, T. E. Angelini, K. Rajendran, C. Y. Park, X. Serra-Picamal, E. H. Zhou, M. H. Zaman, J. P. Butler and D. A. Weitz, *Nat. Mater.*, 2011, **10**, 469–475.
  - [9] G. Helminger, P. A. Netti, H. C. Lichtenbeld, R. J. Melder and R. K. Jain, *Nat. Biotech.*, 1997, **15**, 778–783.
  - [10] S. Kumar and V. M. Weaver, *Cancer Metastasis Rev.*, 2009, **28**, 113–127.
  - [11] R. A. Foty, C. M. Pflieger, G. Forgacs and M. S. Steinberg, *Development*, 1996, **122**, 1611–1620.
  - [12] T. Lecuit, *Trends Cell. Biol.*, 2005, **15**, 34–42.
  - [13] C. Guillot and T. Lecuit, *Science*, 2013, **340**, 1185–1189.
  - [14] Z. Liu, J. L. Tan, D. M. Cohen, M. T. Yang, N. J. Sniadecki, S. A. Ruiz, C. M. Nelson and C. S. Chen, *Proc. Natl. Acad. Sci. USA*, 2010, **107**, 9944–9949.
  - [15] L.-L. Pontani, I. Jorjadze, V. Viasnoff and J. Brujic, *Proc. Natl. Acad. Sci. USA*, 2012, **109**, 9839–9844.
  - [16] J. A. Åström and M. Karttunen, *Phys. Rev. E*, 2006, **73**, 062301.
  - [17] G. W. Jones and S. J. Chapman, *SIAM Rev.*, 2012, **54**, 52–118.
  - [18] D. Gonzalez-Rodriguez, K. Guevorkian, S. Douezan and F. Brochard-Wyart, *Science*, 2012, **338**, 910–917.
  - [19] J. Kursawe, R. E. Baker and A. G. Fletcher, *J. Theor. Biol.*, 2018, **443**, 66–81.
  - [20] L. A. Fernández, V. Martín-Mayor and P. Verrocchio, *Phys. Rev. Lett.*, 2007, **98**, 085702.
  - [21] D. Frenkel and D. J. Wales, *Nat. Mater.*, 2011, **10**, 410–411.
  - [22] M. Charnley, F. Anderegg, R. Holtackers, M. Textor and P. Meraldi, *PLoS ONE*, 2013, **8**, e66918.
  - [23] V. Hernández-Hernández, D. Rueda, L. Caballero, E. R. Alvarez-Buylla and M. Benítez, *Frontiers Plant Sci.*, 2014, **5**, 265.
  - [24] A. Lesman, J. Notbohm, D. A. Tirrell and G. Ravichandran, *J. Cell. Biol.*, 2014, **205**, 155–162.
  - [25] M. Osterfield, C. A. Berg and S. Y. Shvartsman, *Dev. Cell*, 2017, **41**, 337–348.
  - [26] L. M. Owen, A. S. Adhikari, M. Patel, P. Grimmer, N. Leijnse, M. C. Kim, J. Notbohm, C. Franck and A. R. Dunn, *Mol. Biol. Cell*, 2017, **28**, 1959–1974.
  - [27] W. T. Gibson and M. C. Gibson, in *Curr. Top. Dev. Biol.*, Elsevier BV, 2009, pp. 87–114.

- [28] M. Sadati, N. T. Qazvini, R. Krishnan, C. Y. Park and J. J. Fredberg, *Differentiation*, 2013, **86**, 121–125.
- [29] C. Reichhardt and C. J. Olson Reichhardt, *Phys. Rev. E*, 2014, **90**, 012701.
- [30] B. Palmieri, Y. Bresler, D. Wirtz and M. Grant, *Sci. Rep.*, 2015, **5**, 11745.
- [31] C. Alibert, B. Goud and J.-B. Manneville, *Biol. Cell*, 2017, **109**, 167–189.
- [32] S. Suresh, *Acta Biomater.*, 2007, **3**, 413–438.
- [33] A. V. Nguyen, K. D. Nyberg, M. B. Scott, A. M. Welsh, A. H. Nguyen, N. Wu, S. V. Hohlbauch, N. A. Geisse, E. A. Gibb, A. G. Robertson, T. R. Donahue and A. C. Rowat, *Integr. Biol.*, 2016, **8**, 1232–1245.
- [34] Q. Luo, D. Kuang, B. Zhang and G. Song, *Biochim. Biophys. Acta - General Subjects*, 2016, **1860**, 1953–1960.
- [35] P. Znachor, *Anabaena Planctonica*, 2004, figure with permission from Dr. Znachor.
- [36] J. Josef and A. Braun, *Anabaena Laxa*, 1991, figure with permission from Dr. Juráň.
- [37] R. Kudela, *Anabaena Circinalis*, 2018, Creative Commons copyright. Figure with permission from Dr. Kudela.
- [38] M. Demarteau, *Anabaena Flos-Aquae*, 2011, figure with permission from Dr. Demarteau/Aquon.
- [39] F. Pilot and T. Lecuit, *Dev. Dyn.*, 2005, **232**, 685–694.
- [40] M. C. Gibson, A. B. Patel, R. Nagpal and N. Perrimon, *Nature*, 2006, **442**, 1038–1041.
- [41] A. Herrero, J. Stavans and E. Flores, *FEMS Microbiol. Rev.*, 2016, **40**, 831–854.
- [42] J.-Y. Zhang, G.-M. Lin, W.-Y. Xing and C.-C. Zhang, *Frontiers Microbiol.*, 2018, **9**, 791.
- [43] A. Mkrtchyan, J. Åström and M. Karttunen, *Soft Mat.*, 2014, **10**, 4332–4339.
- [44] F. Graner and J. Glazier, *Phys. Rev. Lett.*, 1992, **69**, 2013–2016.
- [45] D. B. Staple, R. Farhadifar, J.-C. Röper, B. Aigouy, S. Eaton and F. Jülicher, *Eur. Phys. J. E*, 2010, **33**, 117–127.
- [46] D. A. Fletcher and R. D. Mullins, *Nature*, 2010, **463**, 485–492.
- [47] R. M. H. Merks and J. A. Glazier, *Physica A*, 2005, **352**, 113–130.
- [48] T. E. Angelini, A. C. Dunn, J. M. Urueña, D. J. Dickrell, D. L. Burris and W. G. Sawyer, *Faraday Disc.*, 2012, **156**, 31.
- [49] Y. Wang, W.-C. Lo and C.-S. Chou, *PLoS Comput. Biol.*, 2017, **13**, e1005843.
- [50] E. Flores, A. Herrero, K. Forchhammer and I. Maldener, *Trends Microbiol.*, 2016, **24**, 79–82.
- [51] G. T. Eisenhoffer, P. D. Loftus, M. Yoshigi, H. Otsuna, C.-B. Chien, P. A. Morcos and J. Rosenblatt, *Nature*, 2012, **484**, 546–549.
- [52] J. Jose, A. van Blaaderen and A. Imhof, *Phys. Rev. E*, 2016, **93**, 062901.
- [53] M. J. Erikson, N. W. Mueggenburg, H. M. Jaeger and S. R. Nagel, *Phys. Rev. E*, 2002, **66**, 2093707.
- [54] A. R. T. van Eerd, W. G. Ellenbroek, M. van Hecke, J. H. Snoeijer and T. J. H. Vlugt, *Phys. Rev. E*, 2007, **75**, 060302.
- [55] H. A. Vinutha and S. Sastry, *Nat. Phys.*, 2016, **12**, 578–583.
- [56] K. D. Nyberg, K. H. Hu, S. H. Kleinman, D. B. Khismatullin, M. J. Butte and A. C. Rowat, *Biophys. J.*, 2017, **113**, 1574–1584.



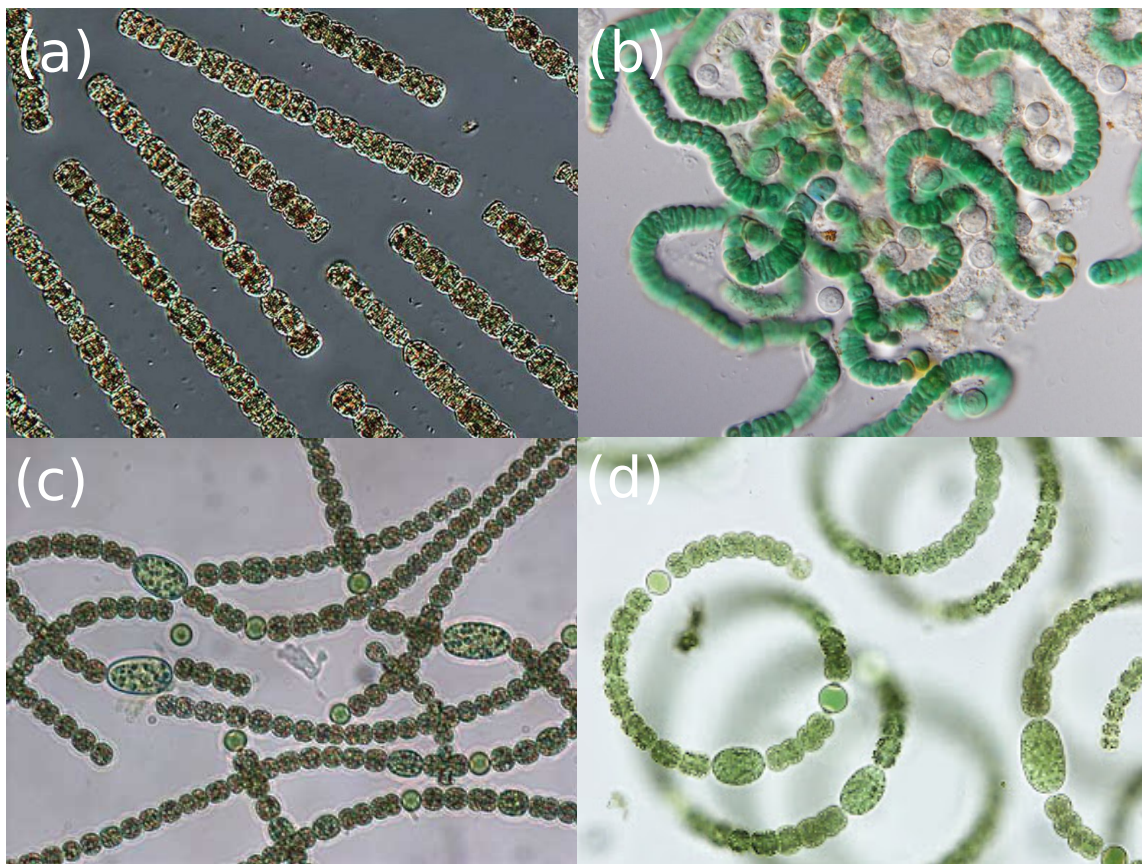


FIG. 1: a) *A. planctonica*. Image with permission from the Laboratory of Phytoplankton Ecology [35]. b) *A. laxa*. Image with permission from the A. Braun Culture Collection of Autotrophic Organisms [36]. c) *A. circinalis*. Image with permission from the Kudela Lab, University of California Santa Cruz [37]. d) *A. flos-aquae*. Image with permission from Demarteau/Aquon [38].

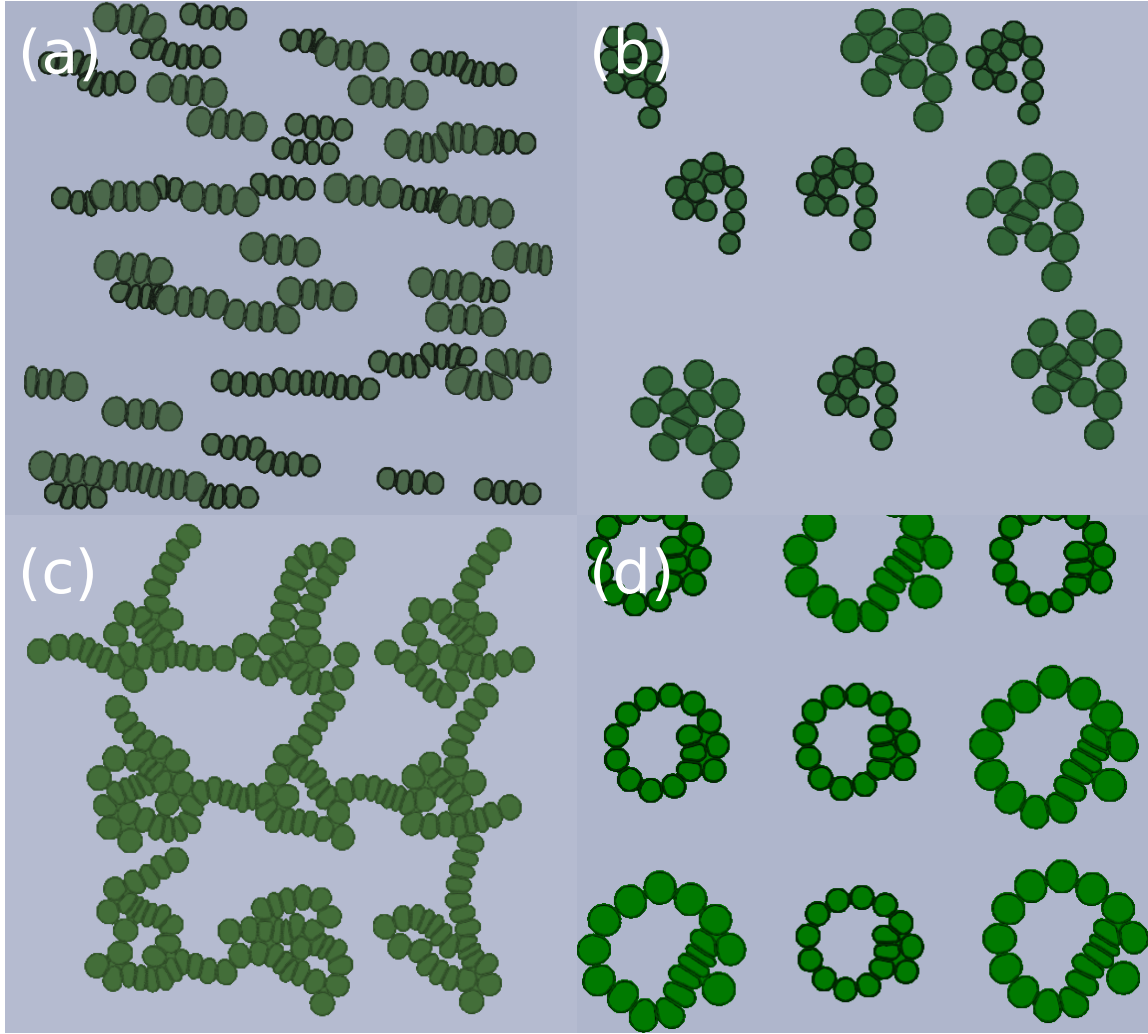


FIG. 2: The type of cell can be changed by changing the division plane choosing rules. a) Division planes parallel at each generation, b) division plane turning left at an increasing rate, c) small clusters of original cells dividing at perpendicular and constant orientation angles, and d) division plane turning left at constant rate.

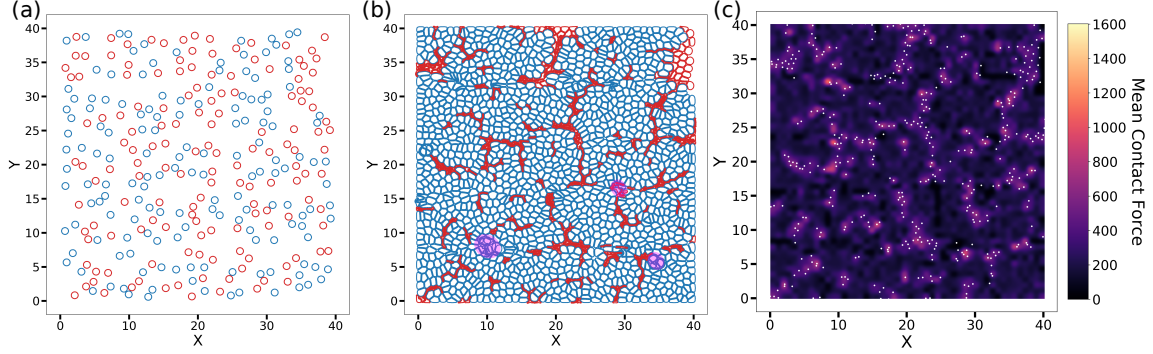


FIG. 3: a) Initial configuration. Stiff cells are depicted in red, and soft in blue. Growth is simulated from this state until confluence. b) A confluent tissue soft and stiff cells. Stiff cells form dendrite or vein-like structures in a matrix of soft cells. The regions marked with light purple are areas where cells interpenetrate and cell death could occur — though death is not simulated by CeDEM. c) Contact force distribution in the same tissue. Large contact forces are located at stiff cells and at boundaries between soft and stiff cells. White markers are the centres of masses of the stiff cells.

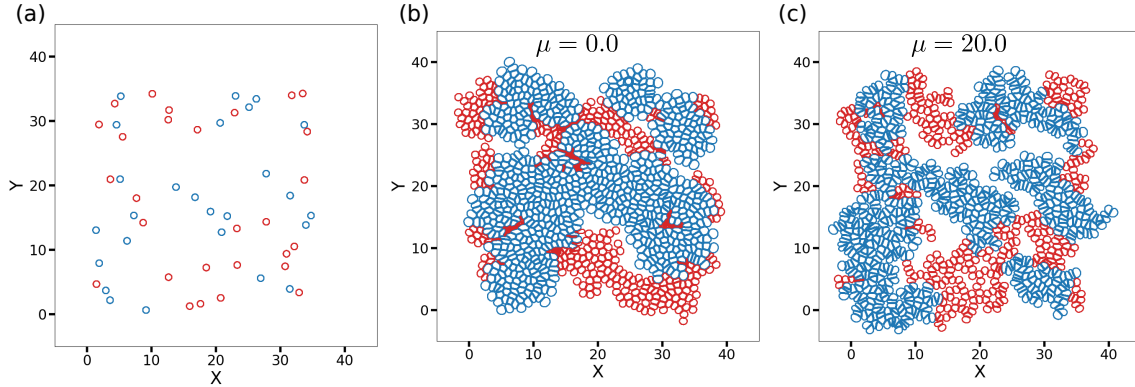


FIG. 4: Morphologies of simulated cells with different inter-cellular friction. a) Initial conditions stiff cells are in red and soft cells in blue. The two are in equal proportions. b) Morphology of zero inter-cellular friction cells. c) Tissue with high-friction cells ( $\mu = 20.0$ ). Both cases were simulated for a time corresponding to 10 division cycles.

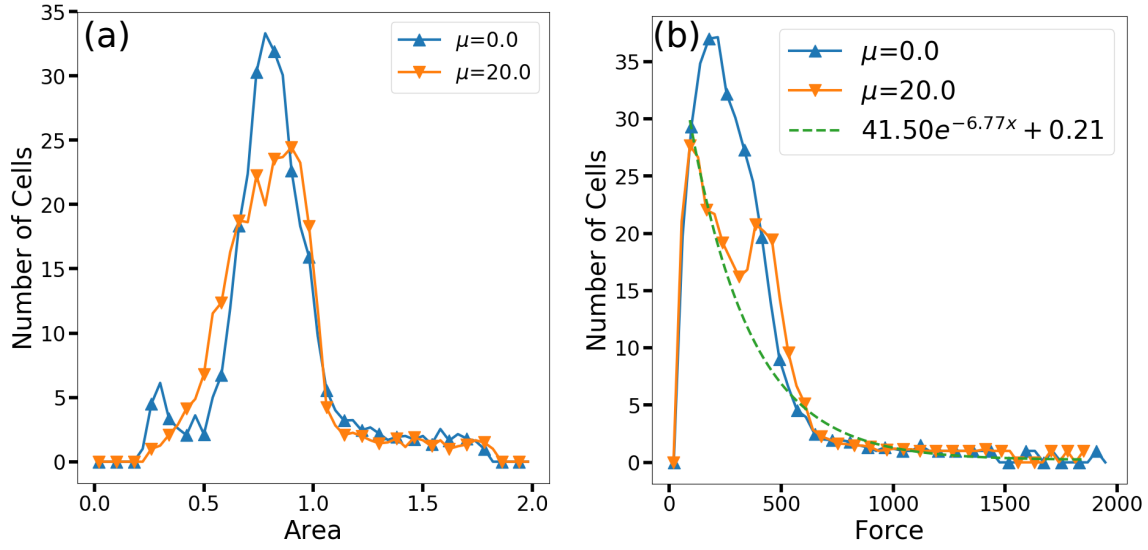


FIG. 5: a) Number distributions of cell areas. There is a peak at low areas corresponding to collapsed stiff cells. b) Number distribution of inter-cell forces at high friction ( $\mu = 20.0$ ) and low friction ( $\mu = 0.0$ ). The green dashed line is an exponential fit to the  $\mu = 20.0$  case, ignoring the second peak.

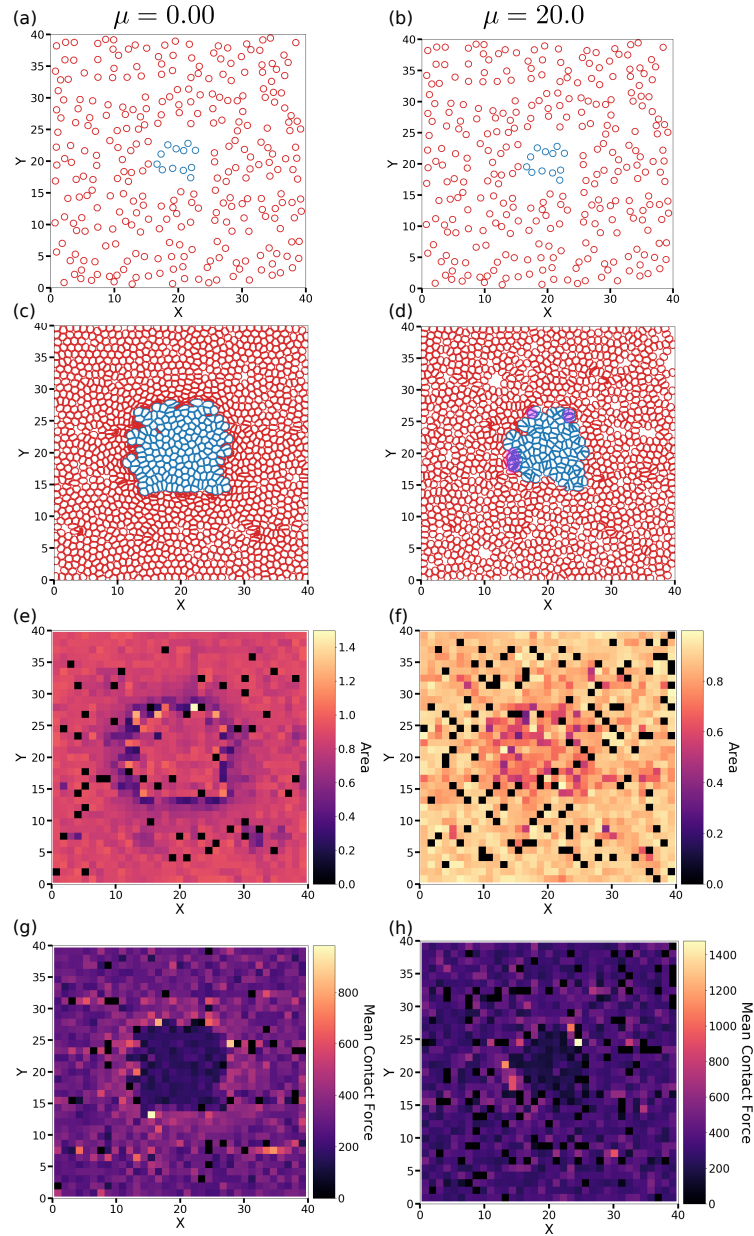


FIG. 6: a) Inclusion of *Type2* (blue) cells in a matrix of *Type1* (red) cells,  $\mu = 0.0$ , b)  $\mu = 20.0$ . c) ,d) configurations for the two cases at confluence. e) Spatial cell size distribution,  $\mu = 0.0$ , f)  $\mu = 20.0$ . g) Spatial contact forces distribution  $\mu = 0.0$ , h)  $\mu = 20.0$ . Black squares: voids in e)–h).

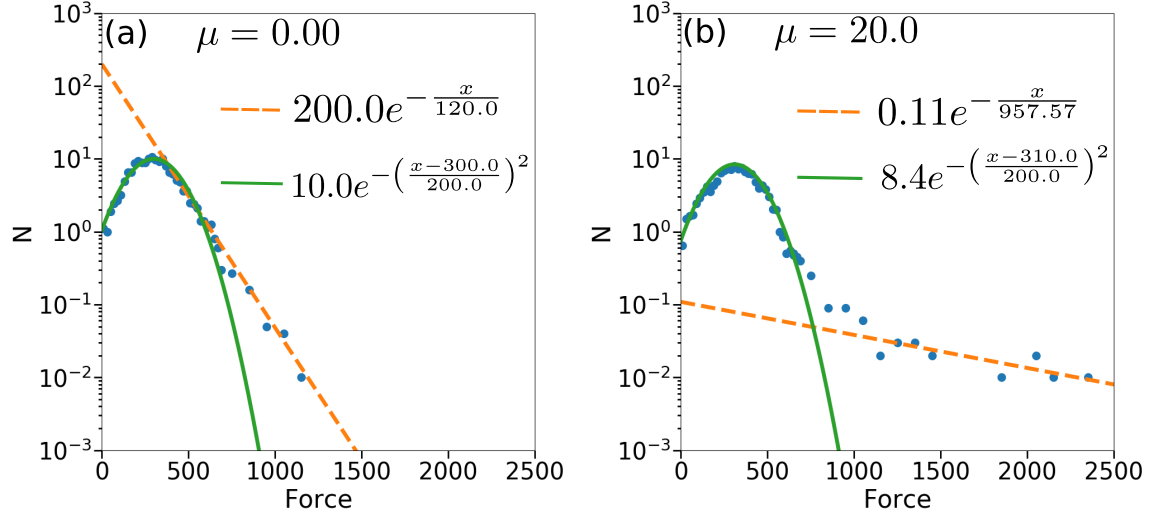


FIG. 7: Distributions of inter-cellular forces when a soft *Type2* cell is introduced into a tissue consisting of stiff *Type1* cells. a)  $\mu = 0.0$  and b)  $\mu = 20.0$ . The distribution of both is similar except the  $\mu = 20.0$  case is slightly wider at forces between 0-1000 and there is a smaller number of cells in b) that experience high forces. See the text for a detailed discussion and relation to jamming.